# Simulation-assisted learning of open quantum systems

Ke Wang<sup>1,\*</sup> and Xiantao Li<sup>1,†</sup>

<sup>1</sup>Department of Mathematics, Pennsylvania State University
(Dated: July 11, 2023)

Models for open quantum systems, which play important roles in electron transport problems and quantum computing, must take into account the interaction of the quantum system with the surrounding environment. Although such models can be derived in some special cases, in most practical situations, the exact models are unknown and have to be calibrated. This paper presents a learning method to infer parameters in Markovian open quantum systems from measurement data. One important ingredient in the method is a direct simulation technique of the quantum master equation, which is designed to preserve the completely-positive property with guaranteed accuracy. The method is particularly helpful in the situation where the time intervals between measurements are large. The approach is validated with error estimates and numerical experiments.

#### I. INTRODUCTION

Quantum learning has recently emerged as a field at the intersection of quantum physics and computer science [1–3]. Its primary focus is on the estimation and characterization of energy levels and interaction coefficients within a quantum system. Such effort has become increasingly crucial for characterizing, optimizing, and controlling quantum systems. One particularly explored area is Hamiltonian learning, where the emphasis is to infer the Hamiltonians [4–11], which ultimately determine the system's energy spectrum and dynamic behavior. Compared to direct simulation approaches, the learning process attempts to map observation data back to the model parameters. An important extension of Hamiltonian learning is the parameter identification of open quantum systems [12, 13], ones that continuously interact with their environment [14]. The ultimate goal is to reconstruct the interactions in the Lindblad-Gorini-Kossakowski-Sudarshan quantum master equation (QME) [15, 16]:

$$\frac{d}{dt}\rho = -i[H,\rho] + \sum_{j=1}^{N_V} (V_j \rho V_j^{\dagger} - \frac{1}{2} V_j^{\dagger} V_j \rho - \frac{1}{2} \rho V_j^{\dagger} V_j), \tag{1}$$

where H is the system Hamiltonian and  $V_j$ 's are jump operators that arise from the interactions with the environment [14].

In practice, the learning tasks are usually formulated as an optimization problem, which is then solved by an iterative method, and as such, one needs to frequently access the objective function, e.g., through the expectations of some observables. The ability to acquire such quantities might be limited by the measurement capabilities. Furthermore, the availability of the gradient of the objective function, a necessary ingredient for a fast optimization algorithm, might not be attainable through experiments either. In this paper, we propose a simulation-assisted method to address these issues. In contrast to the equation-based methods [12, 13] to identify Lindbladians in (1),

<sup>\*</sup> wangke.math@psu.edu

<sup>†</sup> Xiantao.Li@psu.edu

we formulate a trajectory-based framework, where the observations  $A(t) = \operatorname{tr}(Ae^{t\mathcal{L}}\rho(0))$  are fit by simulating the QME (1). An important consequence is that the dependence of accuracy on the measurement time-lapse  $\Delta t$  is replaced by the dependence on the time step  $\delta t$  of the simulation. This offers the flexibility to achieve an accuracy not limited by experimental setups. For example, when the measurement time  $\Delta t$  is large, the numerical simulations fill the gap by generating the solution of the QME (1) in between. Another advantage is that, unlike the equation-based approaches [12, 13], our optimization problem does not require the expectations associated with the right hand side of Eq. (1).

To enable such a simulation-assisted approach, we propose a simulation algorithm, denoted here by  $\mathcal{M}_{\delta t}(t)$ , that has global error  $\delta t^2$ , in that  $e^{\mathcal{L}t} - \mathcal{M}_{\delta t}(t) = \mathcal{O}\left(\delta t^2\right)$ . We choose a semi-implicit algorithm, which is stable even when the coherent term in the QME (1) has large coefficients. This makes it more robust in practice than the second-order method in Breuer and Petruccione [14]. Furthermore, we also show that the method has a completely positive property and it can be easily written in a Kraus form. This makes it possible to implement such a simulation method on a quantum computer as well. This is done by unraveling the Lindblad dynamics to a stochastic Schrödinger equation [14], followed by a stochastic expansion [17].

Another practical aspect of our approach is efficient optimization. With the Kraus representation of our numerical approximation, the calculation of the gradient is streamlined. This allows us to apply the Levenberg- Marquardt algorithm, which has very rapid convergence [18, 19]. With mild assumptions on the fitting error, we will show how the approximation error from the numerical simulation and the statistical error from the measurements affect the performance of the parameter identification.

The rest of the paper is organized as follows: We present a general learning framework in the form of a nonlinear least squares problem in Section II A, and explain the difference and connections to existing works in Section II B. Section II C and Section II D present the specific simulation method and how it is integrated with the optimization procedure. In Section II E and Section III, we present some error analysis and results from some numerical experiments.

# II. THE LEARNING FRAMEWORK FOR PARAMETER IDENTIFICATION OF LINDBLADIANS

#### A. A Least Squares Formulation of the Learning Problem

In practice, the unknown parameter can appear in both the Hamiltonian and the dissipative terms in the QME (1). To indicate the role of the parameters, we first rewrite Eq. (1) as follows,

$$\frac{d}{dt}\rho = \mathcal{L}_{H}(\boldsymbol{\theta}_{H})\rho + \mathcal{L}_{D}(\boldsymbol{\theta}_{D})\rho,$$

$$\mathcal{L}_{H}(\boldsymbol{\theta}_{H})\rho = -i[H, \rho], \quad \mathcal{L}_{D}(\boldsymbol{\theta}_{D})\rho = \sum_{j=1}^{N_{V}} \left(V_{j}\rho V_{j}^{\dagger} - \frac{1}{2}V_{j}^{\dagger}V_{j}\rho - \frac{1}{2}\rho V_{j}^{\dagger}V_{j}\right).$$
(2)

We can combine the parameters by writing  $\boldsymbol{\theta} := (\boldsymbol{\theta}_H, \boldsymbol{\theta}_D); \mathcal{L}(\boldsymbol{\theta}) := \mathcal{L}_H(\boldsymbol{\theta}_H) + \mathcal{L}_D(\boldsymbol{\theta}_D)$  will be called the *Lindbladian*. We refer to the two sets of parameters as Hamiltonian and dissipative parameters, respectively. When  $\mathcal{L}_D = 0$ , the problem is reduced to a Hamiltonian learning problem.

We assume that the measurement data is a time series  $y_{k,n}$ ,  $n = 1, 2, \dots, N_T$ , which correspond

to observables  $A^{(k)}, k = 1, \dots, N_O$ , at time instances  $t_n = n\Delta t, \quad 0 \le n \le N_T$ ,

$$y_{k,n} := \operatorname{tr} \left( A^{(k)} \rho(t_n; \boldsymbol{\theta}) \right). \tag{3}$$

We have set  $t_0 = 0$ , and for simplicity we assume a uniform time-lapse  $\Delta t$  between experiments, although the extension to general distributions of measurement times is straightforward. Also indicated in Eq. (3) is the dependence of the solution of (2) on the parameters, i.e.,  $\rho(t_n; \boldsymbol{\theta}) = e^{t_n \mathcal{L}(\boldsymbol{\theta})} \rho(0)$ .

We now formulate the learning problem based on the consistency in Eq. (3), as a least squares problem,

$$\min_{\boldsymbol{\theta}} \phi(\boldsymbol{\theta}),\tag{4}$$

where the objective function is given by,

$$\phi(\boldsymbol{\theta}) = \frac{1}{2N_O N_T} \sum_{\substack{k=1,\dots,N_O\\n=1,\dots,N_T}} \left| y_{k,n} - y_{k,n}^* \right|^2, \quad y_{k,n}^* := \operatorname{tr}\left( A^{(k)} \rho(t_n; \boldsymbol{\theta}^*) \right), \tag{5}$$

Here,  $y_{k,n}^*$  is interpreted as the measurement data with respect to the true, but unknown parameter  $\theta^*$ ;  $\theta^*$  is the solution of the least squares problem, i.e.,  $\theta^* = \operatorname{argmin}\phi(\theta)$ . Due to the typical nonlinear dependence of  $\rho(t_n; \theta)$  on  $\theta$ , the optimization problem is a nonlinear least squares problem [20].

An alternative viewpoint is a maximum likelihood estimate (MLE) from parameter estimation methods for dynamical systems [21]. Namely, the measurement outcome  $y_{k,n}$  comes with a Gaussian noise  $\epsilon_{k,n}$ ,

$$y_{k,n} = \operatorname{tr}(A^{(k)}\rho(t_n;\boldsymbol{\theta})) + \epsilon_{k,n}.$$

Then Eq. (5) is the log-likelihood function.

#### B. Related Works

The QME (1) is an important alternative to study electron transport properties, which are important in material science [22, 23]. Another increasingly important application is quantum computing, where the quantum circuits are subject to environmental noise, and many quantum error mitigation schemes require the knowledge of an error model, i.e., the channel interactions and strength [24–26].

Bairey et al. [12] proposed to learn the coefficients in the QME (1) by acting the steady-state equation on a collection of observables. These equations can thus be rewritten in terms of the expectations by applying the adjoint of the Lindbladians to the observables, leading to equations of Ehrenfest form. For example, by letting  $\langle A \rangle(t) := \operatorname{tr}(A\rho(t))$ , one can derive from Eq. (1),

$$\frac{d}{dt}\langle A\rangle(t) = -i\langle [A,H]\rangle(t) + \sum_{j=1}^{N_V} \left(\langle V_j^{\dagger} A V_j \rangle(t) - \frac{1}{2}\langle A V_j^{\dagger} V_j \rangle(t) - \frac{1}{2}\langle V_j^{\dagger} V_j A \rangle(t)\right). \tag{6}$$

The operators on the right-hand side can be expressed on a known basis with unknown parameters, which reformulate the equation in terms of measurement data and parameter values. At a

steady state, the time derivative drops out, and the approach by Bairey et al. [12] yields a system of equations, usually over-determined, for the unknown parameters. Franca et al. [13] extended this framework to dynamics problems, with the time derivatives estimated from polynomial approximations. As alluded to in the previous section, these two approaches can be summarized as equation-based: in that the objective function is set up so that the equation (6) holds the best it can. An important practical issue is that the time interval for the measurements, denoted in this article by  $\Delta t$ , might be large, in which case, the accuracy of the inference is limited by the approximation of the time derivatives. Another challenge is that the right hand side of (6) may involve many expectations that have to be obtained from measurements. It is also worthwhile to mention that Boulant et al. [27] also proposed numerical algorithms for reconstructing Lindblad operators and highlighted the importance of the CP property. But their method to ensure this property is quite involved.

The more recent work [28] aims at reconstructing Lindbladians based on measurements at multiple times with an optimization problem. Their method is based on experimental measurements and the least squares problem is formulated in terms of the discrete probability induced by the observables. Numerical simulations are only used to determine a stopping criterion. Compared to this experiment-based approach, the simulation-assisted approach only works with the original set of measurement data. More importantly, the numerical simulation provides the gradient of the objective function, which can substantially speed up the optimization process.

While the equation-based methods [12, 13] fundamentally differ from the method presented in this paper, the two approaches can be combined to accelerate the parameter estimation procedure. Indeed, the current problem can be viewed, in the broader context, as parameter estimation of ODEs [21], where the polynomial approximation of derivatives is known as polynomial regression. It has been used as a preparation of a two-step estimation procedure [29, 30]. The parameters obtained from the linear regression, e.g., in the approach of Franca et al. [13] can be used as an initial guess for a trajectory-based approach.

#### C. Computing the Objective Function using Direct Simulations of the QME

Solving the optimization problem in (4) requires access to the expectation of  $A^{(k)}$  for an approximate parameter  $\theta$ , and such data are unavailable from experiments. This is treated by an efficient numerical algorithm for solving the QME (2). Here we outline a simple derivation of numerical methods, which can be implemented on either classical or quantum computers.

In a nutshell, to approximate the solution operator  $e^{\mathcal{L}t}$  of the QME (1), a simulation-assisted algorithm uses an approximation  $\mathcal{M}_{\delta t}(t)$  and minimizes the difference between  $e^{\mathcal{L}^{\dagger}(t_n)}A$  and  $\mathcal{M}^{\dagger}_{\delta t}(t_n)A$ , by taking the trace with  $\rho(0)$ . Another advantage of this approach is that we no longer have to measure the terms on the right-hand side, as was done in [12, 13]. Thus the number of measurements can be significantly reduced.

The QME encodes a trace-preserving and completely positive (TPCP) map [15, 16], which in the Kraus form, can be generally written as [31] (Choi-Kraus'theorem),

$$\rho_{n+1} = \mathcal{K}[\rho_n] := \sum_j F_j \rho_n F_j^{\dagger}, \tag{7}$$

where  $\sum_{j} F_{j}^{\dagger} F_{j} = I[14]$ . Therefore, if such a Kraus form associated with the solution  $e^{t_{n}\mathcal{L}(\boldsymbol{\theta})}$  of the QME (2) can be found, then the objective function in Eq. (5) and its gradient can be directly evaluated to carry out the optimization task. Another interesting aspect is that this procedure

also places the problem in the general framework of learning a quantum system [3]. Boulant et al. [27] have demonstrated that the CP property increases the overall robustness of the parameter estimation procedure.

Our approach starts by first unraveling the Lindblad equation (2) into the stochastic Schrödinger equation [14],

$$d |\psi(t)\rangle = \left(-iH |\psi(t)\rangle - \frac{1}{2} \sum_{j=1}^{N_V} V_j^{\dagger} V_j |\psi(t)\rangle\right) dt + \sum_{j=1}^{N_V} V_j |\psi(t)\rangle dW_{j;t}$$
 (8)

Here  $|\psi(t)\rangle$  represents a stochastic realization of a quantum state  $\rho(t)$ , in the sense that,

$$\rho(t) = \mathbb{E}[|\psi(t)\rangle\langle\psi(t)|]. \tag{9}$$

In the stochastic equation,  $W_{j;t}$ 's are independent Brownian motions that incorporate the noise from the bath.

Although in practice the trace-preserving property can be ensured by simple scaling, the completely positive property is often destroyed by classical ODE methods [32]. The equivalence between the QME (1) and Eq. (9) is the key ingredient for constructing an approximation of the QME that preserves the CP property. As a quick demonstration, we first consider a time discretization of the stochastic Schrödinger equation (8) by the semi-implicit Euler method [17]. Toward this end, we define numerical time steps,  $\tau_m = m\delta t, m = 0, 1, \dots, M$ , and an approximate wave function  $|\psi_m\rangle$ ,

$$|\psi(\tau_m)\rangle \approx |\psi_m\rangle, \ m \ge 0.$$
 (10)

It is important to point out that the step size  $\delta t$  is a numerical parameter, and it can be much smaller than the measurement time  $\Delta t$ . In order for the simulation to produce expectations at the same time steps as the experiments, choose  $\delta t$  such that,

$$L = \frac{\Delta t}{\delta t} \in \mathbb{N}, \quad M = LN_T. \tag{11}$$

The semi-implicit Euler method follows a time-marching step and implements an iteration formula for  $|\psi_m\rangle$  as follows,

$$|\psi_{m+1}\rangle = |\psi_m\rangle + G|\psi_{m+1}\rangle \,\delta t + \sum_{j=1}^{N_V} V_j |\psi_m\rangle \,\delta W_{j,m}. \tag{12}$$

The terminology "semi-implicit" comes from the treatment of the noise: It is only sampled from the current time step and if  $V_j = 0$ , this method is the standard implicit Euler method for an ordinary differential equation. In Eq. (12)  $\delta W_{j,m}$ 's are independent Gaussian random variables with mean zero and variance  $\delta t$ . In addition, the matrix G is given by,

$$G = -iH - \frac{1}{2} \sum_{j=1}^{N_V} V_j^{\dagger} V_j.$$
 (13)

It also appears in the structure-preserving scheme [32].

We can express the method in a compact form

$$|\psi_{m+1}\rangle = (I - G\delta t)^{-1} \left[ I + \sum_{j=1}^{N_V} V_j \delta W_{j,m} \right] |\psi_m\rangle.$$
 (14)

At this point, an approximation method for the density operator  $\rho$  can easily be obtained. Specifically, let  $\rho_m = \mathbb{E}[|\psi_m\rangle\langle\psi_m|], m \geq 0$ ;  $\rho(\tau_m) \approx \rho_m$ . By taking expectations of (14), we arrive at,

$$\rho_{m+1} = (I - G\delta t)^{-1} \rho_m (I - G\delta t)^{-\dagger} + (I - G\delta t)^{-1} \sum_{j=1}^{N_V} V_j \rho_m V_j^{\dagger} (I - G\delta t)^{-\dagger} \delta t.$$
 (15)

Here we have used  $\mathbb{E}[\delta W_{j,m}] = 0$  and  $\mathbb{E}[\delta W_{j,m} \delta W_{k,m}] = \delta t \delta_{j,k}$ .

Clearly, this can be written in the Kraus form (7). The corresponding Kraus operators are given by,

$$F_0 = (I - G\delta t)^{-1},\tag{16}$$

$$F_j = (I - G\delta t)^{-1} V_j \sqrt{\delta t}, j = 1, \cdots, N_V.$$
(17)

This Kraus form from the semi-implicit Euler method is summarized in Lemma 1.

**Lemma 1.** The semi-implicit Euler method induces a Kraus form, i.e.,  $\rho_{m+1} = \mathcal{K}[\rho_m] = \sum_j F_j \rho_m F_j^{\dagger}$  where  $\sum_j F_j^{\dagger} F_j = I + \mathcal{O}(\delta t^2)$ . In addition,

$$e^{\delta t \mathcal{L}(\boldsymbol{\theta})} \rho - \mathcal{K}\rho = \mathcal{O}(\delta t^2).$$
 (18)

The approximation property can be verified by direct expansions of the Kraus operators in Eq. (16).

In practice, such first-order methods have limited accuracy. To ensure better performance, we consider the second-order implicit approximation method for stochastic differential equations [17, Chapter 15]. When applied to Eq. (8), the method can be written as,

$$|\psi_{m+1}\rangle = (I - \frac{1}{2}G\delta t)^{-1}(I + \frac{1}{2}G\delta t)|\psi_{m}\rangle + \sum_{j=1}^{N_{V}}(I - \frac{1}{2}G\delta t)^{-1}(V_{j} + \frac{1}{2}V_{j}G\delta t)|\psi_{m}\rangle\delta\hat{W}_{j} + \frac{1}{2}(I - \frac{1}{2}G\delta t)^{-1}\sum_{j_{1},j_{2}=1}^{N_{V}}V_{j_{2}}V_{j_{1}}|\psi_{m}\rangle\left(\delta\hat{W}_{j_{1},m}\delta\hat{W}_{j_{2},m} + U_{j_{1},j_{2},m}\right).$$
(19)

In this expression,  $\delta \hat{W}$  is an approximation of an increment of the Brownian motion. In addition,  $U_{j_1,j_2}$  are independent two-point distribution, defined as,

$$P(U_{j_1,j_2} = \pm \delta t) = \frac{1}{2}, \forall j_2 = 1, \dots, j_1 - 1,$$

$$U_{j_1,j_1} = -\delta t,$$

$$U_{j_1,j_2} = -U_{j_2,j_1}, \text{ for } j_2 = j_1 + 1, \dots, N_V, j_1 = 1, \dots, N_V,$$

$$(20)$$

We now state the approximation property of this method.

**Lemma 2.** The implicit second-order approximation induces a Kraus form, i.e.  $\rho_{m+1} = \sum_j F_j \rho_m F_j^{\dagger}$ , where  $\sum_j F_j F_j^{\dagger} = I + \mathcal{O}(\delta t^3)$ . In addition, the one-step error is given by,

$$e^{\delta t \mathcal{L}} \rho = \sum_{j} F_{j} \rho F_{j}^{\dagger} + \mathcal{O}(\delta t^{3}).$$
 (21)

*Proof.* Similar to Lemma 1, we define  $\rho_m = \mathbb{E}[|\psi_m\rangle \langle \psi_m|]$ . Following the second-order implicit scheme (19), each iteration of the density operator is as follows,

$$\rho_{m+1} = (I - \frac{1}{2}G\delta t)^{-1}(I + \frac{1}{2}G\delta t)\rho_{m}(I + \frac{1}{2}G\delta t)(I - \frac{1}{2}G\delta t)^{-1} 
+ (I - \frac{1}{2}G\delta t)^{-1}\sum_{j=1}^{N_{V}}V_{j}(I + \frac{1}{2}G\delta t)\rho_{m}(I + \frac{1}{2}G\delta t)V_{j}^{\dagger}(I - \frac{1}{2}G\delta t)^{-1}\delta t 
+ \frac{1}{2}(I - \frac{1}{2}G\delta t)^{-1}\sum_{j_{1},j_{2}=1}^{N_{V}}V_{j_{1}}V_{j_{2}}\rho_{m}V_{j_{2}}^{\dagger}V_{j_{1}}^{\dagger}(I - \frac{1}{2}G\delta t)^{-1}(\delta t)^{2} 
= \sum_{j=0}^{N_{V}^{2}+N_{V}}F_{j}\rho_{m}F_{j}^{\dagger} =: \mathcal{K}(\rho_{m})$$
(22)

where the Kraus operators are given by,

$$F_{0} = (I - \frac{1}{2}G\delta t)^{-1}(I + \frac{1}{2}G\delta t),$$

$$F_{j} = (I - \frac{1}{2}G\delta t)^{-1}V_{j}(I + \frac{1}{2}G\delta t)\sqrt{\delta t}, j = 1, \dots, N_{V},$$

$$F_{j_{1}+N_{V}j_{2}} = \frac{1}{\sqrt{2}}(I - \frac{1}{2}G\delta t)^{-1}V_{j_{1}}V_{j_{2}}\delta t, \quad j_{1}, j_{2} = 1, \dots, N_{V}.$$

$$(23)$$

Notice that the one-step error is of the third order, so we can simplify the iteration formula without changing the error order by letting

$$F_{j_1+N_V j_2} = \frac{1}{\sqrt{2}} V_{j_1} V_{j_2} \delta t, \quad j_1, j_2 = 1, \cdots, N_V.$$
 (24)

This will simplify the calculation of the gradient. The rest of the proof is given in Appendix A 2.

We choose an implicit method due to its numerical stability. For example, one can show that the spectral radius of each Kraus operator has an upper bound that is independent of H. This can be seen from the observation that the real part of the matrix G is positive definite. Therefore, the spectral radius of  $F_0$  is less or equal to 1. For  $0 < j \le N_V$ ,  $F_j$  has a spectral radius less or equal to the spectral radius of  $V_j \sqrt{\delta t}$ .

#### D. Gradient Evaluations for Gradient-based Optimization

The problem of finding the optima of  $\phi(\theta)$  can be seen as the nonlinear least squares problem

$$\phi(\boldsymbol{\theta}) = \frac{1}{2N_O N_T} \sum_{\substack{k=1,\dots,N_O\\n=1,\dots,N_T}} |r_{k,n}(\boldsymbol{\theta})|^2 = \frac{1}{2N_O N_T} R(\boldsymbol{\theta})^T R(\boldsymbol{\theta}), \tag{25}$$

where we used the textbook notations [20]:  $r_{k,n} = y_{k,n} - y_{k,n}^*$  is the residual error and  $R(\boldsymbol{\theta}) = (r_{k,n})_{k,n}$  will be referred to as the residual vector. We are interested in the scenario when the dimension of the residual is larger than the number of parameters, i.e., the over-determined regime.

One practical iteration method for solving the least squares problem is the Levenberg-Marquardt (LM) algorithm, which, starting with an initial guess,  $\boldsymbol{\theta}^{(0)}$ , involves updating the parameters iteratively,

$$\boldsymbol{\theta}^{(k+1)} - \boldsymbol{\theta}^{(k)} = -\left(\nu_k I + R'(\boldsymbol{\theta}^{(k)})^T R'(\boldsymbol{\theta}^{(k)})\right)^{-1} R'(\boldsymbol{\theta}^{(k)})^T R(\boldsymbol{\theta}^{(k)}). \tag{26}$$

It can be seen as a combination of the Gauss-Newton method and the gradient descent algorithm. In Eq. (26), R' denotes the gradient of the residual with respect to the parameters. The parameter  $\nu_k$  serves as a regularization, and in practice, it can be chosen to be proportional to the norm of the residual error.

The convergence of the LM method has been established under very mild conditions. Here we follow [18, 19] and pose the following local condition: There exists a constant C, such that,

$$||R(\boldsymbol{\theta})|| \ge C||\boldsymbol{\theta} - \boldsymbol{\theta}^*||, \tag{27}$$

for all  $\theta$  in a neighborhood of  $\theta^*$ .

**Theorem 1.** [18, Theorem 2.1] Assume that Eq. (27) holds and R' is Lipschitz continuous. Let the parameter  $\nu_k$  be

$$\nu_k = \left\| R(\boldsymbol{\theta}^{(k)}) \right\|^2.$$

If the initial guess  $\theta^{(0)}$  is sufficiently close to  $\theta^*$ , then there exists a constant, such that the iterations from (26) satisfy,

$$\left\|\boldsymbol{\theta}^{(k+1)} - \boldsymbol{\theta}^*\right\| \le C \left\|\boldsymbol{\theta}^{(k)} - \boldsymbol{\theta}^*\right\|^2. \tag{28}$$

The convergence speed is faster than the super-linear convergence proved in [20]. The quadratic convergence property makes the LM method (26) an extremely useful algorithm. Global convergence has also been analyzed in [18, 19]. This is often accomplished by using a line search algorithm.

In parameter estimation problems, the condition in Eq. (27) is viewed as a local identifiability condition [21]. Meanwhile, the Lipschitz condition can be verified by assuming that the first order and second derivatives of  $\mathcal{L}(\boldsymbol{\theta})$  are bounded, which holds trivially if the Lindbladian has a linear dependence on the parameters. To elaborate on this, a partial derivative of the residual error is given by,

$$\frac{\partial}{\partial \theta_{\alpha}} r_{k,n}(\boldsymbol{\theta}) = \operatorname{tr}(A^{(k)} \partial_{\theta_{\alpha}} \rho(t_n; \boldsymbol{\theta})). \tag{29}$$

This leads us to consider  $\Gamma_{\alpha}(t, \boldsymbol{\theta}) := \partial_{\theta_{\alpha}} \rho(t; \boldsymbol{\theta})$ , which from Eq. (2), follows the differential equation,

$$\frac{d}{dt}\Gamma_{\alpha}(t,\boldsymbol{\theta}) = \mathcal{L}(\boldsymbol{\theta})\Gamma_{\alpha}(t,\boldsymbol{\theta}) + \frac{\partial}{\partial\theta_{\alpha}}\mathcal{L}(\boldsymbol{\theta})\rho(t,\boldsymbol{\theta}).$$

Using the contraction property of  $e^{t\mathcal{L}}$  [33], we find that,

$$\|\Gamma_{\alpha}(t,\boldsymbol{\theta})\| \leq t \|\partial_{\theta_{\alpha}}\mathcal{L}(\boldsymbol{\theta})\|.$$

To examine the Lipschitz continuity of the partial derivatives, we define,

$$\chi_{\alpha,\beta} := \partial_{\theta_{\beta}} \Gamma_{\alpha}(t, \boldsymbol{\theta}),$$

which follows the equation,

$$\frac{d}{dt}\chi_{\alpha,\beta}(t,\boldsymbol{\theta}) = \mathcal{L}(\boldsymbol{\theta})\chi_{\alpha,\beta}(t,\boldsymbol{\theta}) + \frac{\partial^2}{\partial\theta_{\beta}\partial\theta_{\alpha}}\mathcal{L}(\boldsymbol{\theta})\rho(t,\boldsymbol{\theta}) + \frac{\partial}{\partial\theta_{\alpha}}\mathcal{L}(\boldsymbol{\theta})\Gamma_{\beta}(t,\boldsymbol{\theta}) + \frac{\partial}{\partial\theta_{\beta}}\mathcal{L}(\boldsymbol{\theta})\Gamma_{\alpha}(t,\boldsymbol{\theta}),$$

and a simple bound follows.

$$\|\chi_{\alpha,\beta}(t,\boldsymbol{\theta})\| \leq t \left\| \frac{\partial^2}{\partial \theta_{\alpha} \partial \theta_{\beta}} \mathcal{L}(\boldsymbol{\theta}) \right\| + \frac{t^2}{2} (2\|\partial_{\theta_{\alpha}} \mathcal{L}(\boldsymbol{\theta})\| + \|\partial_{\theta_{\beta}} \mathcal{L}(\boldsymbol{\theta})\|).$$

As a result, if the first and second order derivatives of  $\mathcal{L}(\theta)$  are bounded, R' fulfills the Lipschitz condition.

Meanwhile, in our learning task, the residual function is subject to approximation and statistical error. To incorporate these errors, we first state a generalization of the convergence result, which can be proved by following the proof in [18],

**Proposition 1.** Let  $\epsilon > 0$ . Suppose that the residual vector R is subject to an  $\epsilon$  perturbation,

$$R \to R + \Delta R$$
.

with  $||\Delta R|| \leq \epsilon$ , for all  $\boldsymbol{\theta}$  in a neighborhood of  $\boldsymbol{\theta}^*$ , and assume that  $\Delta R'$  is Lipschitz continuous as well. Then the LM iterations, under the same conditions on R as in the previous theorem, exhibit an approximate quadratic convergence,

$$\left\|\boldsymbol{\theta}^{(k+1)} - \boldsymbol{\theta}^*\right\| \le C \left\|\boldsymbol{\theta}^{(k)} - \boldsymbol{\theta}^*\right\|^2 + \epsilon. \tag{30}$$

The LM algorithm in Eq. (26) requires access to the gradient of the residual function. To facilitate the calculation of the gradient, we first take the derivative of the Kraus form,

$$(\partial_{\theta} \mathcal{K})[\rho] = \sum_{j} \partial_{\theta} F_{j} \rho F_{j}^{\dagger} + F_{j} \rho \partial_{\theta} F_{j}^{\dagger}$$
(31)

Here  $\theta$  refers to one parameter in  $\theta$ . The entire gradient can be computed by visiting all the components in  $\theta$ . For clarity, we express the results as an inner product in the space of Hermitian matrices. Namely, for any Hermitian matrices A and B, we define,

$$\langle A, B \rangle := \operatorname{tr}(AB).$$
 (32)

Now we show how the gradient of the objective function can be computed from a back propagation procedure.

**Lemma 3.** Assume that the iteration  $\rho_m \to \rho_{m+1}$  follows a Kraus form,

$$\rho_{m+1} = \mathcal{K}\rho_m := \sum_j F_j \rho_m F_j^{\dagger}. \tag{33}$$

Then, for any Hermitian operator A, the following identify holds,

$$\langle A, \rho_{m+1} \rangle = \langle \mathcal{K}^* A, \rho_m \rangle, \tag{34}$$

where,  $K^*$  stands for the adjoint of K. Namely,

$$\mathcal{K}^*[A] := \sum_j F_j^{\dagger} A F_j. \tag{35}$$

*Proof.* By the cyclic property of the trace operator, we have

$$\operatorname{tr}(A\rho_{m+1}) = \sum_{j} \operatorname{tr}\left(AF_{j}\rho_{m}F_{j}^{\dagger}\right) = \sum_{j} \operatorname{tr}\left(F_{j}^{\dagger}AF_{j}\rho_{m}\right) = \operatorname{tr}(\mathcal{K}^{*}[A]\rho_{m})$$

In light of this Lemma, we have,

**Theorem 2.** When the density operator is simulated by the form of  $\rho_{m+1} = \mathcal{K}[\rho_m] := \sum_j F_j \rho_m F_j^{\dagger}$  for each simulation time step  $\delta t$ , the explicit form of the derivative of the objective function  $\phi(\boldsymbol{\theta})$  can be written as

$$\partial_{\theta_{\alpha}} \phi(\boldsymbol{\theta}) = \frac{1}{N_O N_T} \sum_{k=1}^{N_O} \sum_{n=1}^{N_T} \sum_{l=1}^{nL} \left( y_{k,n} - y_{k,n}^* \right) \left\langle \partial_{\theta_{\alpha}} \mathcal{K}^* A_{nL-l}^{(k)}, \ \rho_{nL-l} \right\rangle, \tag{36}$$

where  $A_{nL-l}^{(k)} := (\mathcal{K}^*)^{l-1}[A^{(k)}]$  can be viewed as a back-propagated operator.

*Proof.* The detailed proof can be found in Appendix A1.

By using Theorem 2, the explicit expression of  $\partial_{\theta_{\alpha}}\phi(\theta)$  can be obtained once we know the derivative of  $F_j$ . For instance, for the first-order semi-implicit Euler method,

$$\partial_{\theta} F_{0} = F_{0} \partial_{\theta} G F_{0} \delta t$$
  

$$\partial_{\theta} F_{j} = \partial_{\theta} F_{0} V_{j} \sqrt{\delta t} + F_{0} \partial_{\theta} V_{j} \sqrt{\delta t}, j = 1, \cdots, N_{V}$$
(37)

Similarly, for the second-order implicit approximation (22), we have,

$$\partial_{\theta} F_{0} = \frac{1}{2} \delta t (I - \frac{1}{2} G \delta t)^{-1} \partial_{\theta} G(F_{0} + I)$$

$$\partial_{\theta} F_{j} = \frac{1}{2} \delta t (I - \frac{1}{2} G \delta t)^{-1} \partial_{\theta} G F_{j} + \sqrt{\delta t} (I - \frac{1}{2} G \delta t)^{-1} \partial_{\theta} V_{j} (I + \frac{1}{2} G \delta t)$$

$$+ \frac{1}{2} \delta t^{3/2} (I - \frac{1}{2} G \delta t)^{-1} V_{j} \partial_{\theta} G, \quad j = 1, \dots, N_{V}$$

$$\partial_{\theta} F_{j_{1} + N_{V} j_{2}} = \frac{\delta t}{\sqrt{2}} (\partial_{\theta} V_{j_{1}} V_{j_{2}} + V_{j_{1}} \partial_{\theta} V_{j_{2}}), \quad j_{1}, j_{2} = 1, \dots, N_{V}$$
(38)

#### E. Quantifying the Error in the Parameter Identification

Similar to modern machine learning problems, there are mainly three sources of error in a quantum learning problem. Specifically, as can be seen from the objective function Eq. (5),

1. The estimated values,  $\operatorname{tr}(A^{(k)}\rho(t_n;\boldsymbol{\theta}))$  are replaced with  $\operatorname{tr}(A^{(k)}\rho_{nL}(\boldsymbol{\theta}))$  (Recall that  $\Delta t = L\delta t$ , and  $\rho(t_n,\boldsymbol{\theta}) = \rho(\tau_{Ln},\boldsymbol{\theta}) \approx \rho_{Ln}(\boldsymbol{\theta})$ ). This can be regarded as a function approximation error. To include this error, we define,

$$\widehat{r}_{k,n}(\boldsymbol{\theta}) = \operatorname{tr}(A^{(k)}\rho_{nL}(\boldsymbol{\theta})) - y_{k,n}^*. \tag{39}$$

Using the second-order method (22),  $\widehat{R} = (\widehat{r}_{k,n})_{k,n}$  is a  $\mathcal{O}(\delta t^2)$  perturbation of the residual error in the original objective function (5).

2. The data  $y_{k,n}^*$ , as indicated in (3), come from measuring a set of observables at different time instances, which are subject to statistical error. To clarify this perspective, we express the measurement values as random variables:

$$y_{k,n}^* \approx \hat{y}_{k,n} := \frac{1}{N_S} \sum_{\ell=1}^{N_S} a_{k,n,\ell}.$$
 (40)

 $N_S$  indicates the number of times the measurements are repeated. The effect of this sampling error can be understood by considering the following objective function,

$$\widetilde{r}_{k,n}(\boldsymbol{\theta}) = \operatorname{tr}(A^{(k)}\rho(t_n,\boldsymbol{\theta})) - \hat{y}_{k,n}.$$
(41)

Based on Chebyshev's inequality,  $\widetilde{R} = (\widetilde{r}_{k,n})_{k,n}$  is a  $\epsilon$  perturbation of residual error in the original objective function (5) with high probability if  $N_S = \mathcal{O}(1/\epsilon^2)$ .

3. The optimization problem (4) may lead to a nonlinear system of equations and we may not be able to find the exact solution after a finite number of iterations. This is the optimization error.

The perturbation caused by the numerical approximation (22) is a deterministic perturbation, which from (27), causes a perturbation of the identified parameter.

**Theorem 3.** Under the assumption (27), there exists a  $\delta_0 > 0$ , such that for all  $\delta t < \delta_0$ , there is a minimizer  $\hat{\boldsymbol{\theta}}$  of the least squares problem defined by the residual vector in Eq. (39), such that

$$\left\|\hat{\boldsymbol{\theta}} - \boldsymbol{\theta}^*\right\| \le C\delta t^2. \tag{42}$$

for some constant C.

We now turn to the measurement error. Since the observables  $A^{(k)}$ 's are bounded, the measurement noise is bounded, and they can be regarded as a sub-Gaussian random variable. The Hoeffding inequality [34] implies that,

**Lemma 4.** There exists  $\sigma_{k,n}$ , such that the following inequality holds for every  $\epsilon > 0$ 

$$\mathbb{P}\left(\left|\hat{y}_{k,n} - y_{k,n}^*\right| > \epsilon\right) \le 2e^{-\frac{N_S \epsilon^2}{\sigma_{k,n}^2}}.$$
(43)

Now by using a union bound, we can estimate the probability,

$$\mathbb{P}\left(\sqrt{\sum_{k,n} \left| \hat{y}_{k,n} - y_{k,n}^* \right|^2} > \epsilon\right) \le 2N_O N_T e^{-\frac{N_S \epsilon^2}{N_O N_T \sigma^2}}.$$

Here we have set  $\sigma^2 = \frac{1}{N_O N_T} \sum_{k,n} \sigma_{k,n}^2$ .

**Theorem 4.** Under the same assumption as in the previous theorem, and further assume that the observation data  $y_{k,n}$  are sampled,

$$N_S = \Omega\left(\frac{\sigma^2 N_O N_T}{\epsilon^2} \log\left(N_O N_T\right)\right),\tag{44}$$

times, then there is a minimizer  $\widetilde{\boldsymbol{\theta}}$  of the nonlinear least squares with residual in Eq. (41), such that

$$\left\|\widetilde{\boldsymbol{\theta}} - \boldsymbol{\theta}^*\right\| \le \epsilon. \tag{45}$$

with high probability.

#### III. NUMERICAL TESTS

#### A. Phase Damping Model with Linear Parameter Dependence

We first consider an N-spin system with dephasing and amplitude damping noise on every qubit [24]. The dynamics are described by the QME in Eq. (1), with the parametric form of the Hamiltonian part given by,

$$H = \sum_{j=1}^{N} H_{j}, \quad H_{j} = \sum_{\alpha=1}^{3} e_{j,\alpha} \sigma_{j}^{\alpha} + \sum_{\alpha,\beta=1}^{3} c_{j,\alpha,\beta} \sigma_{j}^{\alpha} \sigma_{j+1}^{\beta}, \quad j = 1, \dots, N.$$
 (46)

 $\sigma_j^{\alpha}$  is the Pauli matrix  $\sigma^{\alpha}$  ( $\alpha=x,y,z$ ) applied to the jth qubit, and we choose  $c_{N,\alpha,\beta}=0$  to model an open boundary condition.

Meanwhile, the dissipation term is parameterized as follows,

$$\mathcal{L}_D \rho = \lambda_1 \sum_{j=1}^N \mathcal{T}[\sigma_j^-] \rho + \lambda_2 \sum_{j=1}^N \mathcal{T}[\sigma_j^z] \rho, \tag{47}$$

where the operator  $\mathcal{T}[V]$  is defined as

$$\mathcal{T}[V]\rho = V\rho V^{\dagger} - \frac{1}{2} \{ V^{\dagger} V, \rho \}. \tag{48}$$

In Eq. (47) we defined operators  $\sigma_j^{\pm} := 2^{-1}(\sigma_j^x \pm i\sigma_j^y)$ . The density operator  $\rho(0)$  is initialized as a product state with all spins up.

In this example, the parameter  $\boldsymbol{\theta}$  is composed of Hamiltonian coefficients  $\boldsymbol{\theta}_H = \{e_{j,\alpha}, c_{j,\alpha,\beta}\}$  and dissipative parameters  $\boldsymbol{\theta}_D = (\lambda_1, \lambda_2)$ . Specifically, there are 65 unknown parameters when N = 6.

These parameters will be generated from a Gaussian distribution, and then held fixed as the exact values of the parameters.

We first test the accuracy of the simulation methods in Section II C. As a reference, we conducted direct simulations of the test model in Eqs. (46) and (47) by using very small step size:  $\delta t = 10^{-4}$ , and we compute the 1-qubit local observable  $A := \sigma_2^y$ . This solution will be regarded as the exact solution  $y_{\text{exact}}(t)$  for comparison purposes. Fig. 1 shows the history of this observable in the time interval  $t \in [0, 10]$ . Also shown is the solution computed from the semi-implicit Euler method (15) and the second-order implicit method (22) using step size  $\delta t = 10^{-2}$ , with solutions denoted as  $y_1(t)$ , and  $y_2(t)$ , respectively. One can observe that the semi-implicit Euler's method yields very good accuracy in the initial period [0,0.5], but only a qualitatively correct solution in the transient state [0.5,4]. In addition, it tends to smear out the solution in the long run, e.g., in the final period [6,10]. But the second-order implicit method offers much better accuracy in the entire time duration. Due to the high accuracy, the measurement data in the following numerical experiments will be generated using the second-order implicit method with  $\delta t = 10^{-2}$ .

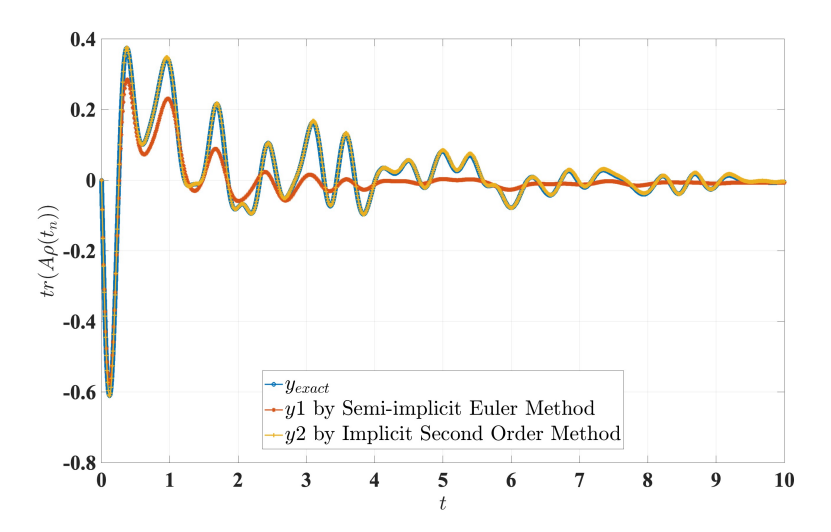


FIG. 1: Comparison of the accuracy for the simulation methods in Section II C. We consider a chain of 6 spins with dephasing and amplitude damping noise in this section. The density operator  $\rho$  is measured with 1-qubit local observables  $A := \sigma_2^y$  and we denoted the measurement as  $y_n = \operatorname{tr}(A\rho(t_n))$ . The blue solid line represents the "exact" solution generated with a very small step size.

Now we test the optimization algorithms in Section II D with the objective function (5) computed from simulations of the Lindblad equation. We consider observable time  $t_n = 0.1, 0.2, \dots, 1$  with measurement interval  $\Delta t = 0.1$  and simulation interval  $\delta t = 0.01$ : L = 10. In addition, we test the algorithms by choosing  $A^{(k)}$ 's as the basis of all 1-local observables or all 2-local observables generated by Pauli matrices. The optimization results are displayed in ??. To indicate the progress of the optimization, we show the value of the objective function as well as the relative error:  $\|\theta - \theta^*\|/\|\theta^*\|$ . We observe that the optimization using the Levenberg-Marquardt algorithm (26) converges very quickly. In addition, the optimization problem (5) using all 2-local observables leads

to a slightly faster parameter identification.

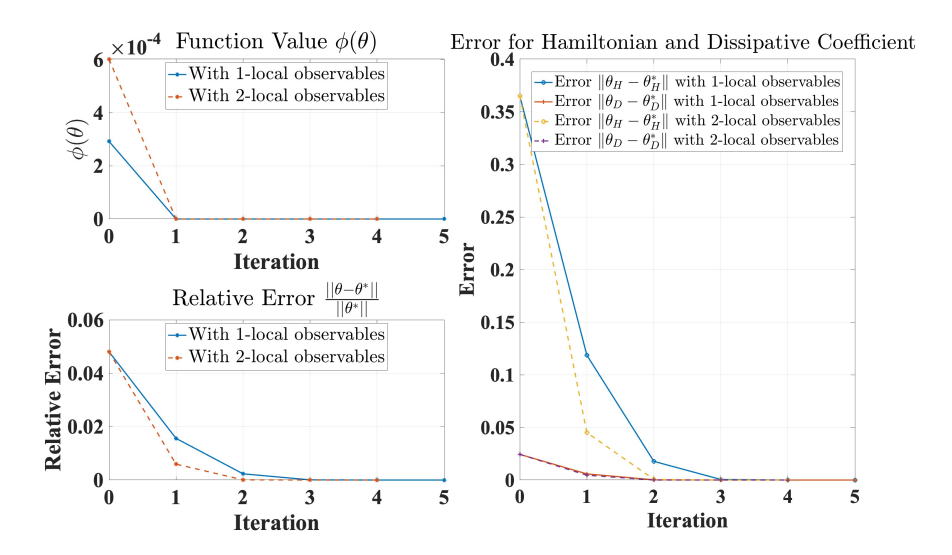


FIG. 2: Reconstruction of the Lindbladians in Eqs. (46) and (47) by solving the optimization problem (5). In terms of  $y_{k,n}$  in (3), we consider two cases: one with all 1-local observables  $(N_O = 19)$ , and the other with all 2-local observables  $(N_O = 154)$ . The initial parameter  $\boldsymbol{\theta}^{(0)}$  is randomly selected with initial error  $\|\boldsymbol{\theta}^{(0)} - \boldsymbol{\theta}^*\| = 0.3658$ . The observable time is  $t_n = 0.1, 0.2, \dots, 1$  with measurement interval  $\Delta t = 0.1$  and numerical simulation time difference  $\delta t = 0.01$ .

We see from the previous experiment that having more observables can improve the identification of the parameters. In the next experiment, we keep the 1-local observables, but increase the number of measurements in time instead. Specifically, we set the observation time to  $t=0.01,0.02,\cdots,1$ , i.e.,  $\Delta t=\delta t=0.01$ . From Fig. 3, we observe that these more frequent measurements also improve the identification of the parameters slightly: The optimization converged in fewer steps. The efficiency of the optimization can again be attributed to the rapid convergence of the LM algorithm.

Our last experiment is motivated by the study in [12], where the coefficients in the Lindbladians are learned after the system reaches a steady state. To do this, we choose the observation time at a later stage  $t = 4.1, 4.2, \dots, 5$ , and a separate numerical test verified that this is when the system is beginning to saturate (see Fig. 1 as well). We see from Fig. 4 that the optimization is still able to identify all the parameters. In particular, the parameters  $\theta_H$  do not converge monotonically. But the last few iterations converged very fast.

#### B. A Nonlinear parametric model

In this section, we consider a test problem similar to the ones considered in Bairey et al. [12]. The model has the same parametric form for the Hamiltonian terms (46). However, the jump operators

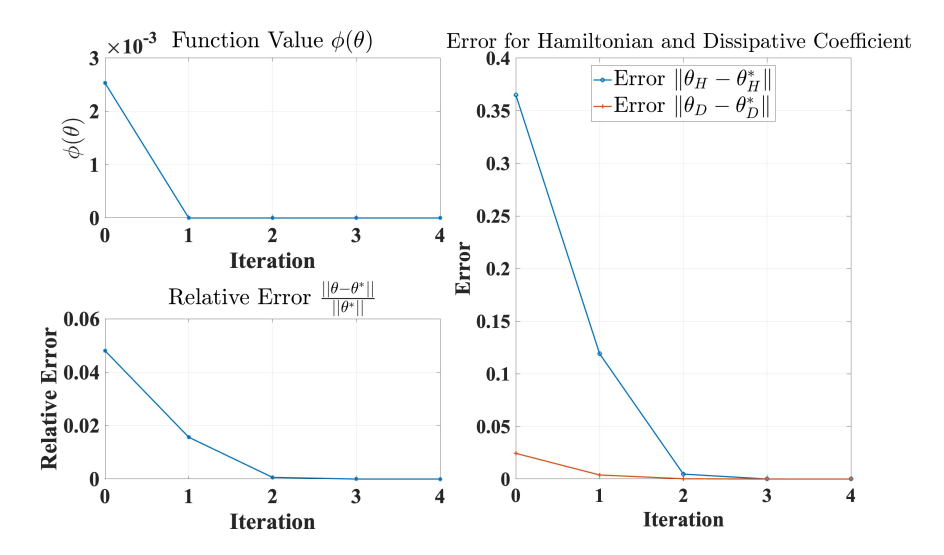


FIG. 3: Reconstruction of the Lindbladians in Eqs. (46) and (47) by solving the optimization problem (5). In terms of  $y_{k,n}$  in (3), we consider all 1-local observables ( $N_O=19$ ) and set the observation time to  $t=0.01,0.02,\cdots,1$ , i.e. the measurement interval  $\Delta t=0.01$  ( $N_T=100$ ). The simulation time interval  $\delta t=0.01$ . The initial parameter  $\boldsymbol{\theta}^{(0)}$  is the same as ??.

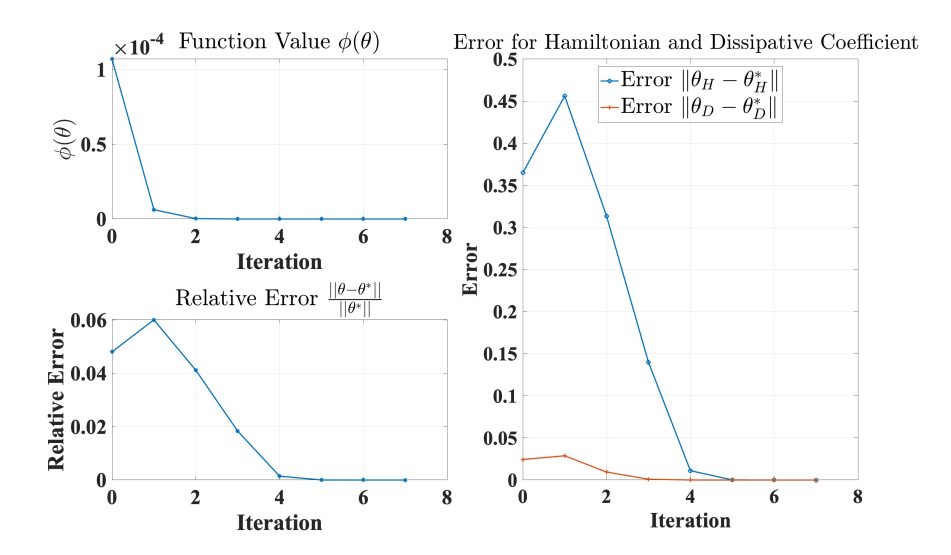


FIG. 4: Reconstruction of the Lindbladians in Eqs. (46) and (47) by solving the optimization problem (5). In terms of  $y_{k,n}$  in (3), we consider all 1-local observables ( $N_O=19$ ) and set the observation time to  $t=4.1,4.2,\cdots,5,~(N_T=10)$ . And the simulation time interval  $\delta t=0.01$ . The initial parameter  $\boldsymbol{\theta}^{(0)}$  is the same as ??.

are expanded as a linear combination of local Pauli matrices,

$$V_{j} = \sum_{\alpha=1}^{3} d_{j,\alpha} \sigma_{j}^{\alpha} = \sum_{\alpha=1}^{3} d_{j,\alpha}^{(1)} \sigma_{j}^{\alpha} + i d_{j,\alpha}^{(2)} \sigma_{j}^{\alpha}, \quad j = 1, \dots, N_{V}.$$

$$(49)$$

This parametric form is clearly more general. In particular, the Lindbladian is a *nonlinear* function of the parameters.

We first choose these dissipative parameters randomly according to a Gaussian distribution, specifically,

$$e_{j,\alpha}, c_{j,\alpha,\beta} \sim \mathcal{N}(0,1), \quad \text{Re}(d_{j,\alpha}), \text{Im}(d_{j,\alpha}) \sim \mathcal{N}(0,\frac{1}{2}).$$
 (50)

These parameters will then be fixed and considered to be exact. Subsequently, they are used to generate the observation data  $y_{k,n}^*$  in (3). We have noticed that the parametric form in Eq. (50) is not unique due to the simultaneous appearance of  $V_j$  and  $V_j^{\dagger}$  in the Lindbladian. To eliminate the redundancy from a global phase of  $d_j$  for each j, we let

$$d_{j,1} = d_{j,1}^{(1)}, \quad j = 1, \dots, N_V,$$
 (51)

which means that the imaginary part  $d_{j,1}^{(2)} = 0$ . The parameter  $\boldsymbol{\theta}$  is composed by Hamiltonian part  $\boldsymbol{\theta}_H = \{e_{j,\alpha}, c_{j,\alpha,\beta}\}$  as in Eq. (46) in the previous test problem, as well as the dissipation part of the parameter is  $\boldsymbol{\theta}_D = \{d_{j,\alpha}^{(1)}, d_{j,\alpha}^{(2)}\}$ .

We consider the optimization problem (5) with values  $y_{k,n}^*$  computed from 1-local and 2-local observables at time  $t=0.1,0.2,\cdots,1$ . The measurement time interval is thus  $\Delta t=0.1$ , while the simulation time interval is much smaller:  $\delta t=0.01$ . In our numerical test, the randomly chosen initial guess for the optimization has an error  $\|\boldsymbol{\theta}^{(0)} - \boldsymbol{\theta}^*\| = 0.4529$ . We then run the optimization algorithm. The results are summarized in Fig. 5. Although the Lindblad operator is a nonlinear function of the parameters, the optimization problem still identifies the parameters rather quickly. Also observed is that with all 2-local observables, the optimization converges faster. One speculation is that the constant in the condition (27) is larger for the choice with all 2-local observables.

To further test the effect of the choice of the observables, we choose 1-local observables, by only keeping  $\sigma_j^x$  and  $\sigma_j^y$ 's for each spin, while other configurations of the test remain the same. In this case, we observe that the optimization takes many more iterations to reach a plateau, as shown in Fig. 6, and the optimization error is still quite large, indicating that this collection of observables are inadequate for the Lindbladian learning problem.

# IV. SUMMARY AND DISCUSSIONS

In this paper, we presented an algorithm to infer parameters in an open quantum system, specifically, in a Lindblad equation. Rather than working with the observation times, we introduce smaller time scales where the solution is obtained by direct numerical simulations. There are two advantages. On one hand, since the objective function is formulated based on trajectories, we no longer need the observables that correspond to the Lindbladian terms that appeared in the approach in [12, 13]. As a result, the number of observables can be much less than the number of jump operators. On the other hand, the algorithm enables flexible control of the accuracy by using smaller step sizes in the numerical simulation.

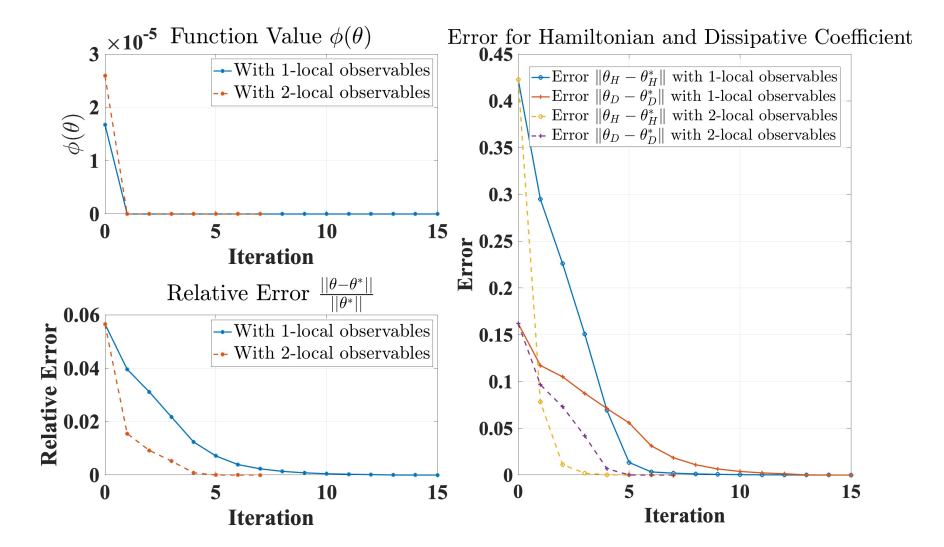


FIG. 5: Reconstruction of the Lindbladians in Eqs. (46) and (49) by solving the optimization problem (5). In terms of  $y_{k,n}$  in (3), we consider two cases: one with all 1-local observables  $(N_O=19)$ , and the other with all 2-local observables  $(N_O=154)$ . The measurement time interval  $\Delta t=0.1$  and the step size for the simulation is  $\delta t=0.01$ . The initial parameter  $\boldsymbol{\theta}^{(0)}$  is randomly selected with initial error  $\|\boldsymbol{\theta}^{(0)}-\boldsymbol{\theta}^*\|=0.4529$ .

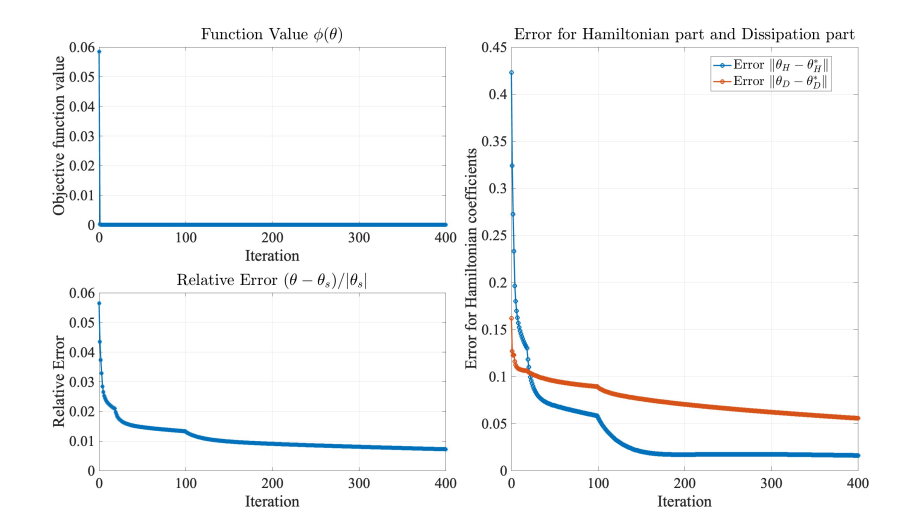


FIG. 6: Reconstruction of the Lindbladians in Eqs. (46) and (49) by solving the optimization problem (5). In terms of  $y_{k,n}$  in (3), we consider fewer 1-local observables  $\sigma_j^x, \sigma_j^y$  ( $N_O = 12$ ) and measurement time  $t = 0.1, 0.2, \dots, 1$  ( $N_T = 10$ ) with simulation time interval  $\delta t = 0.01$ . The initial parameter  $\boldsymbol{\theta}^{(0)}$  is the same as the previous test.

Due to the close relation with quantum computing, one natural question is whether we can use quantum algorithms to perform the simulation of the Lindblad equation, especially when the dimension is too large for simulations on classical computers. The idea of simulating Lindblad dynamics on quantum computers has recently been explored by several groups [35–38]. The existing algorithms can be combined with gradient estimation algorithms to update the parameters in a least squares algorithm, e.g., see [39, 40] for examples of such hybrid schemes. Another alternative is to concatenate Eq. (19) and form a linear system of equations, which can be solved by quantum linear solvers (QLS) [41, 42]. Due to the many technical elements involved in these algorithms, we will present these methods in separate works.

#### ACKNOWLEDGEMENTS

We thank Dr. Di Fang for providing some important references. This work is supported by NSF Grant DMS-1819011 and DMS-2111221.

- [1] M. P. da Silva, O. Landon-Cardinal, and D. Poulin, Practical characterization of quantum devices without tomography, Physical Review Letters 107, 210404 (2011).
- [2] J. Wang, S. Paesani, R. Santagati, S. Knauer, A. A. Gentile, N. Wiebe, M. Petruzzella, J. L. O'brien, J. G. Rarity, A. Laing, et al., Experimental quantum Hamiltonian learning, Nature Physics 13, 551 (2017).
- [3] H.-Y. Huang, S. T. Flammia, and J. Preskill, Foundations for learning from noisy quantum experiments, arXiv preprint arXiv:2204.13691 (2022).
- [4] C. E. Granade, C. Ferrie, N. Wiebe, and D. G. Cory, Robust online Hamiltonian learning, New Journal of Physics 14, 103013 (2012).
- [5] K. Rudinger and R. Joynt, Compressed sensing for Hamiltonian reconstruction, Physical Review A 92, 052322 (2015).
- [6] N. Wiebe, C. Granade, and D. G. Cory, Quantum bootstrapping via compressed quantum Hamiltonian learning, New Journal of Physics 17, 022005 (2015).
- [7] D. Burgarth and A. Ajoy, Evolution-free Hamiltonian parameter estimation through Zeeman markers, Physical Review Letters 119, 030402 (2017).
- [8] A. Sone and P. Cappellaro, Hamiltonian identifiability assisted by a single-probe measurement, Physical Review A 95, 022335 (2017).
- [9] Y. Wang, D. Dong, B. Qi, J. Zhang, I. R. Petersen, and H. Yonezawa, A quantum Hamiltonian identification algorithm: Computational complexity and error analysis, IEEE Transactions on Automatic Control 63, 1388 (2017).
- [10] A. Zubida, E. Yitzhaki, N. Lindner, and E. Bairey, Optimal short-time measurements for Hamiltonian learning, Bulletin of the American Physical Society 67 (2022).
- [11] H.-Y. Huang, Y. Tong, D. Fang, and Y. Su, Learning many-body Hamiltonians with Heisenberg-limited scaling, Physical Review Letters 130, 200403 (2023).
- [12] E. Bairey, C. Guo, D. Poletti, N. H. Lindner, and I. Arad, Learning the dynamics of open quantum systems from their steady states, New Journal of Physics 22, 032001 (2020).
- [13] D. S. Franca, L. A. Markovich, V. Dobrovitski, A. H. Werner, and J. Borregaard, Efficient and robust estimation of many-qubit Hamiltonians, arXiv preprint arXiv:2205.09567 (2022).
- [14] H.-P. Breuer, F. Petruccione, et al., The theory of open quantum systems (Oxford University Press on Demand, 2002).
- [15] G. Lindblad, On the generators of quantum dynamical semigroups, Communications in Mathematical Physics 48, 119 (1976).

- [16] V. Gorini, A. Kossakowski, and E. C. G. Sudarshan, Completely positive dynamical semigroups of N-level systems, Journal of Mathematical Physics 17, 821 (1976).
- [17] P. Kloeden and E. Platen, Numerical Solution of Stochastic Differential Equations, Stochastic Modelling and Applied Probability (Springer Berlin Heidelberg, 2011).
- [18] N. Yamashita and M. Fukushima, On the rate of convergence of the Levenberg-Marquardt method, in *Topics in Numerical Analysis: With Special Emphasis on Nonlinear Problems* (Springer, 2001) pp. 239–249.
- [19] J.-y. Fan and Y.-x. Yuan, On the quadratic convergence of the Levenberg-Marquardt method without nonsingularity assumption, Computing 74, 23 (2005).
- [20] C. T. Kelley, Iterative methods for optimization (SIAM, 1999).
- [21] N. J. Brunel, Parameter estimation of ODE's via nonparametric estimators, Electronic Journal of Statistics 2, 1242 (2008).
- [22] R. Biele and R. D'Agosta, A stochastic approach to open quantum systems, Journal of Physics: Condensed Matter 24, 273201 (2012).
- [23] M. Di Ventra and R. D'Agosta, Stochastic time-dependent current-density-functional theory, Physical Review Letters 98, 226403 (2007).
- [24] K. Temme, S. Bravyi, and J. M. Gambetta, Error mitigation for short-depth quantum circuits, Physical review letters 119, 180509 (2017).
- [25] S. Endo, S. C. Benjamin, and Y. Li, Practical quantum error mitigation for near-future applications, Physical Review X 8, 031027 (2018).
- [26] Z. Cai, R. Babbush, S. C. Benjamin, S. Endo, W. J. Huggins, Y. Li, J. R. McClean, and T. E. O'Brien, Quantum error mitigation, arXiv preprint arXiv:2210.00921 (2022).
- [27] N. Boulant, T. F. Havel, M. A. Pravia, and D. G. Cory, Robust method for estimating the lindblad operators of a dissipative quantum process from measurements of the density operator at multiple time points, Physical Review A 67, 042322 (2003).
- [28] E. B. Av, Y. Shapira, N. Akerman, and R. Ozeri, Direct reconstruction of the quantum-master-equation dynamics of a trapped-ion qubit, Physical Review A 101, 062305 (2020).
- [29] O. Strebel, A preprocessing method for parameter estimation in ordinary differential equations, Chaos, Solitons & Fractals 57, 93 (2013).
- [30] P. Bhaumik and S. Ghosal, Bayesian two-step estimation in differential equation models, Electronic Journal of Statistics 9, 3124 (2015).
- [31] J. Watrous, The theory of quantum information (Cambridge university press, 2018).
- [32] Y. Cao and J. Lu, Structure-preserving numerical schemes for Lindblad equations, arXiv preprint arXiv:2103.01194 (2021).
- [33] M. B. Ruskai, Beyond strong subadditivity? improved bounds on the contraction of generalized relative entropy, Reviews in Mathematical Physics 6, 1147 (1994).
- [34] C. Jin, P. Netrapalli, R. Ge, S. M. Kakade, and M. I. Jordan, A short note on concentration inequalities for random vectors with subgaussian norm, arXiv preprint arXiv:1902.03736 (2019).
- [35] M. Kliesch, T. Barthel, C. Gogolin, M. J. Kastoryano, and J. Eisert, Dissipative quantum Church-Turing theorem, Physical Review Letters 107, 10.1103/physrevlett.107.120501 (2011).
- [36] A. M. Childs and T. Li, Efficient simulation of sparse Markovian quantum dynamics, Quantum Information & Computation 17, 0901 (2017).
- [37] R. Cleve and C. Wang, Efficient quantum algorithms for simulating Lindblad evolution, in 44th International Colloquium on Automata, Languages, and Programming, (ICALP 2017) (2017) pp. 17:1–17:14.
- [38] C. W. Xiantao Li, Simulating Markovian open quantum systems using higher-order series expansion, arXiv preprint arXiv:2212.02051 (2022).
- [39] A. Gilyén, S. Arunachalam, and N. Wiebe, Optimizing quantum optimization algorithms via faster quantum gradient computation, in *Proceedings of the Thirtieth Annual ACM-SIAM Symposium on Discrete Algorithms* (SIAM, 2019) pp. 1425–1444.
- [40] X. Li and C. Wang, Efficient quantum algorithms for quantum optimal control, arXiv preprint arXiv:2304.02613 (2023).
- [41] A. W. Harrow, A. Hassidim, and S. Lloyd, Quantum algorithm for solving linear systems of equations, Physical Review Letters 103, 150502 (2009), arXiv: 0811.3171.

[42] A. M. Childs, R. Kothari, and R. D. Somma, Quantum algorithm for systems of linear equations with exponentially improved dependence on precision, SIAM Journal on Computing 46, 1920 (2017).

### Appendix A: Appendix

## 1. Proof of Theorem 2

*Proof.* The derivative of the objective function  $\phi$  is of the form

$$\partial_{\theta_{\alpha}} \phi(\boldsymbol{\theta}) = \frac{1}{N_O N_T} \sum_{k=1}^{N_O} \sum_{n=1}^{N_T} (y_{k,n} - y_{k,n}^*) \langle A^{(k)}, \partial_{\theta_{\alpha}} \rho(\tau_{nL}; \boldsymbol{\theta}) \rangle$$
(A1)

Let  $\chi_{nL}^{\alpha} = \partial_{\theta_{\alpha}} \rho(\tau_{nL}; \boldsymbol{\theta})$  and  $\rho_{nL} := \rho(\tau_{nL}; \boldsymbol{\theta})$ . The iteration formula for the density operator is of the Kraus form  $\rho_{m+1} = \mathcal{K}[\rho_m] := \sum_j F_j \rho_m F_j^{\dagger}, m = 1, \dots, nL$ . It reveals  $\chi_{m+1}^{\alpha} = \mathcal{K}[\chi_m^{\alpha}] + \partial_{\theta_{\alpha}} \mathcal{K}[\rho_m]$ , then

$$\langle A^{(k)}, \chi_{nL}^{\alpha} \rangle = \langle A^{(k)}, \mathcal{K} \chi_{nL-1}^{\alpha} \rangle + \langle A^{(k)}, \partial_{\theta_{\alpha}} \mathcal{K} \rho_{nL-1} \rangle$$

$$\langle A^{(k)}, \mathcal{K} \chi_{nL-1}^{\alpha} \rangle = \langle A^{(k)}, \mathcal{K}^{2} \chi_{nL-2}^{\alpha} \rangle + \langle A^{(k)}, \mathcal{K} (\partial_{\theta_{\alpha}} \mathcal{K}) \rho_{nL-2} \rangle$$

$$\vdots$$

$$\Rightarrow \langle A^{(k)}, \chi_{nL}^{\alpha} \rangle = \langle A^{(k)}, \mathcal{K}^{nL} \chi_{0}^{\alpha} \rangle + \sum_{l=1}^{nL} \langle A^{(k)}, \mathcal{K}^{l-1} (\partial_{\theta_{\alpha}} \mathcal{K}) \rho_{nL-l} \rangle$$

$$= \sum_{l=1}^{nL} \langle A^{(k)}, \mathcal{K}^{l-1} (\partial_{\theta_{\alpha}} \mathcal{K}) \rho_{nL-l} \rangle$$
(A2)

as  $\chi_0^{\alpha} = 0$ . By taking the adjoint operator,

$$\partial_{\theta_{\alpha}}\phi(\boldsymbol{\theta}) = \frac{1}{N_{O}N_{T}} \sum_{k,n} (y_{k,n} - y_{k,n}^{*}) \sum_{l=1}^{nL} \left\langle (\partial_{\theta_{\alpha}} \mathcal{K})^{*} (\mathcal{K}^{*})^{l-1} A^{(k)}, \rho_{nL-l} \right\rangle$$

$$= \frac{1}{N_{O}N_{T}} \sum_{k,n} (y_{k,n} - y_{k,n}^{*}) \sum_{l=1}^{nL} \left\langle (\partial_{\theta_{\alpha}} \mathcal{K})^{*} A_{nL-l}^{(k)}, \rho_{nL-l} \right\rangle$$
(A3)

where  $A_{nL-1}^{(k)}:=(\mathcal{K}^*)^{l-1}[A^{(k)}]$  is a back-propagated operator and the adjoint Kraus form

$$(\partial_{\theta_{\alpha}} \mathcal{K})^{*}(\rho) = \sum_{j} (\partial_{\theta_{\alpha}} F_{j})^{\dagger} \rho F_{j} + F_{j}^{\dagger} \rho (\partial_{\theta_{\alpha}} F_{j}), \quad \mathcal{K}^{*}(\rho) = \sum_{j} F_{j}^{\dagger} \rho F_{j}$$
(A4)

for real parameters  $\boldsymbol{\theta}$ .

#### 2. Second Order Implicit Approximation Algorithm

Similar to Lemma 1, we start with the unraveled SDE,

$$d|\psi\rangle = (-iH_S|\psi\rangle - \frac{1}{2}\sum_{j=1}^{N_V} V_j^{\dagger} V_j |\psi\rangle) dt + \sum_{j=1}^{N_V} V_j |\psi\rangle dW_{j;t} = G|\psi\rangle dt + \sum_{j=1}^{N_V} V_j |\psi\rangle dW_{j;t}$$
(A5)

According to the second order implicit weak scheme[17, Chapter 15], we can write down a time-marching scheme for the wave function,

$$|\psi_{m+1}\rangle = |\psi_{m}\rangle + \frac{1}{2}(G|\psi_{m+1}\rangle + G|\psi_{m}\rangle)\delta t + \sum_{j=1}^{N_{V}} V_{j} |\psi_{m}\rangle \delta \hat{W}_{j}$$

$$+ \frac{1}{2} \sum_{j=1}^{N_{V}} L^{0}V_{j} |\psi_{m}\rangle \delta \hat{W}_{j}\delta t + \frac{1}{2} \sum_{j_{1},j_{2}=1}^{N_{V}} L^{j_{1}}V_{j_{2}} |\psi_{m}\rangle (\delta \hat{W}_{j_{1}}\delta \hat{W}_{j_{2}} + U_{j_{1},j_{2}}).$$
(A6)

In this expression,  $\delta \hat{W}$  is an approximation of an increment of the Brownian motion. It was suggested in [17] to sample with the three-point distribution,

$$P(\delta \hat{W} = \pm \sqrt{3\Delta}) = \frac{1}{6}, P(\delta \hat{W} = 0) = \frac{2}{3}$$
 (A7)

Meanwhile,  $U_{j_1,j_2}$ 's are independent two-point distributed random variables with

$$P(U_{j_1,j_2} = \pm \Delta) = \frac{1}{2}, \forall j_2 = 1, \dots, j_1 - 1$$

$$U_{j_1,j_1} = -\Delta$$

$$U_{j_1,j_2} = -U_{j_2,j_1}, \text{ for } j_2 = j_1 + 1, \dots, N_V, j_1 = 1, \dots, N_V.$$
(A8)

In Eq. (A6), the diffusion operator  $L^{j_1}$ 's are defined as follows.

$$L^{0}V_{j}|\psi\rangle = \sum_{k=1}^{d} (G\psi)^{k} \frac{\partial}{\partial \psi^{k}} V_{j}|\psi\rangle = \sum_{k=1}^{d} (G\psi)^{k} V_{j}(:,k) = V_{j}G|\psi\rangle$$

$$L^{j_{1}}V_{j_{2}}|\psi\rangle = \sum_{k=1}^{d} (V_{j_{1}}\psi)^{k} \frac{\partial}{\partial \psi^{k}} V_{j_{2}}|\psi\rangle = \sum_{k=1}^{d} (V_{j_{1}}\psi)^{k} V_{j_{2}}(:,k) = V_{j_{2}}V_{j_{1}}|\psi\rangle$$
(A9)

Here the notation (:, k) indicates the kth column of the matrix. Thus, the equation 19 or 22 can be rewritten as

$$|\psi_{m+1}\rangle = (I - \frac{1}{2}G\delta t)^{-1}(I + \frac{1}{2}G\delta t)|\psi_{m}\rangle + \sum_{j=1}^{N_{V}}(I - \frac{1}{2}G\delta t)^{-1}(V_{j} + \frac{1}{2}V_{j}G\delta t)|\psi_{m}\rangle\delta\hat{W}_{j}$$

$$+ \frac{1}{2}(I - \frac{1}{2}G\delta t)^{-1}\sum_{j_{1},j_{2}=1}^{N_{V}}V_{j_{2}}V_{j_{1}}|\psi_{m}\rangle(\delta\hat{W}_{j_{1}}\delta\hat{W}_{j_{2}} + U_{j_{1},j_{2}}).$$
(A10)

By taking expectations, this time-marching scheme induces an iteration formula for the density operator  $\rho_m = \mathbb{E}[|\psi_m\rangle \langle \psi_m|]$ , as follows.

$$\rho_{m+1} = (I - \frac{1}{2}G\delta t)^{-1}(I + \frac{1}{2}G\delta t)\rho_{m}(I + \frac{1}{2}G\delta t)(I - \frac{1}{2}G\delta t)^{-1} 
+ (I - \frac{1}{2}G\delta t)^{-1}\sum_{j=1}^{N_{V}}V_{j}(I + \frac{1}{2}G\delta t)\rho_{m}(I + \frac{1}{2}G\delta t)V_{j}^{\dagger}(I - \frac{1}{2}G\delta t)^{-1}\delta t 
+ \frac{1}{2}(I - \frac{1}{2}G\delta t)^{-1}\sum_{j_{1},j_{2}=1}^{N_{V}}V_{j_{1}}V_{j_{2}}\rho_{m}V_{j_{2}\dagger}V_{j_{1}\dagger}(I - \frac{1}{2}G\delta t)^{-1}(\delta t)^{2} 
= \sum_{j=0}^{N_{V}}F_{j}\rho_{m}F_{j}^{\dagger} + \sum_{j_{1},j_{2}=1}^{N_{V}}A_{j_{1},j_{2}}\rho_{m}A_{j_{1},j_{2}}^{\dagger} 
= \sum_{j=0}^{N_{V}^{2}+N_{V}}F_{j}\rho_{m}F_{j}^{\dagger} = \mathcal{K}[\rho_{m}]$$
(A11)

where the Kraus operator

$$F_{0} = (I - \frac{1}{2}G\delta t)^{-1}(I + \frac{1}{2}G\delta t)$$

$$F_{j} = (I - \frac{1}{2}G\delta t)^{-1}V_{j}(I + \frac{1}{2}G\delta t)\sqrt{\delta t}, j = 1, \dots, N_{V}$$

$$A_{j_{1},j_{2}} = \frac{1}{\sqrt{2}}(I - \frac{1}{2}G\delta t)^{-1}V_{j_{1}}V_{j_{2}}\delta t, j_{1}, j_{2} = 1, \dots, N_{V}$$

$$F_{j_{1}+N_{V},j_{2}} = A_{j_{1},j_{2}}, j_{1}, j_{2} = 1, \dots, N_{V}$$
(A12)

To show that the method has second order accuracy, we first expand the solution of the Lindblad equation (2),

$$\rho(\tau_{m+1}) = \rho(\tau_m) + \delta t \mathcal{L} \rho(\tau_m) + \frac{1}{2} \delta t^2 \mathcal{L}^2 \rho(\tau_m) + \mathcal{O}(\delta t^3). \tag{A13}$$

In particular, we have,

$$\mathcal{L}\rho = -i[H, \rho] + \sum_{j=1}^{N_V} \left( V_j \rho V_j^{\dagger} - \frac{1}{2} \{ V_j^{\dagger} V_j, \rho \} \right).$$

We now show that the method (19) has a consistent expansion at (A13) up to  $\mathcal{O}(\delta t^2)$ . Toward this end, we expand the Kraus operators,

$$F_{0} = I + G\delta t + \frac{1}{2}G^{2}\delta t^{2} + \mathcal{O}(\delta t^{3}),$$

$$F_{j} = V_{j}\sqrt{\delta t} + \frac{1}{2}\{G, V_{j}\}\delta t\sqrt{\delta t} + \frac{1}{2}\{G, GV_{j}\}\delta t^{2}\sqrt{\delta t} + \mathcal{O}(\delta t^{7/2}), \qquad j = 1, \dots, N_{V}$$

$$F_{j_{1}+N_{V}j_{2}} = \frac{1}{\sqrt{2}}V_{j_{1}}V_{j_{2}}\delta t + \mathcal{O}(\delta t^{3/2}), \qquad j_{1}, j_{2} = 1, \dots, N_{V}$$

By substituting these expansions of the jump operators, and only keeping terms of order up to  $\mathcal{O}(\delta t^2)$ , we find that,

$$\rho_{m+1} = \rho_m + \delta t (G\rho_m + \rho_m G^{\dagger}) + \frac{1}{2} \delta t^2 (G^2 \rho_m + 2G\rho_m G^{\dagger} + \rho_m G^{\dagger^2})$$

$$+ \delta t \sum_{j=1}^{N_V} V_j \rho_m V_j^{\dagger} + \frac{1}{2} \delta t^2 \sum_{j=1}^{N_V} \left( V_j \rho_m \{G, V_j\}^{\dagger} + \{G, V_j\} \rho_m V_j^{\dagger} \right)$$

$$+ \frac{1}{2} \delta t^2 \sum_{j_1, j_2 = 1}^{N_V} V_{j_1} V_{j_2} \rho_m V_{j_2}^{\dagger} V_{j_1}^{\dagger} + \mathcal{O}(\delta t^3).$$

In light of Eq. (13), the  $\mathcal{O}(\delta t)$  terms are consistent with that in (A13). With lengthy calculations, we can also see that the  $\mathcal{O}(\delta t^2)$  terms are also consistent. From the calculation of the consistency of  $\mathcal{O}(\delta t)$ , we know that  $G\rho_m + \rho_m G^{\dagger} = \mathcal{L}\rho_m - \sum_j V_j \rho_m V_j^{\dagger}$ . The detailed calculation can be summarized as follows:

$$\begin{split} G^{2}\rho_{m} + 2G\rho_{m}G^{\dagger} + \rho_{m}G^{\dagger^{2}} &= G(G\rho_{m} + \rho_{m}G^{\dagger}) + (G\rho_{m} + \rho_{m}G^{\dagger})G^{\dagger} \\ &= \mathcal{L}^{2}\rho_{m} - \sum_{j=1}^{N_{V}} \mathcal{L}(V_{j}\rho_{m}V_{j}^{\dagger}) - \sum_{j=1}^{N_{V}} V_{j}\mathcal{L}\rho_{m}V_{j}^{\dagger} + \sum_{j_{1},j_{2}=1}^{N_{V}} V_{j_{2}}V_{j_{1}}\rho_{m}V_{j_{1}}V_{j_{2}} \\ &= \sum_{j=1}^{N_{V}} \left(V_{j}\rho_{m}\{G,V_{j}\}^{\dagger} + \{G,V_{j}\}\rho_{m}V_{j}^{\dagger}\right) = \sum_{j} (V_{j}\rho_{m}V_{j}^{\dagger}G^{\dagger} + GV_{j}\rho_{m}V_{j}^{\dagger}) + V_{j}(\rho_{m}G^{\dagger} + G\rho_{m})V_{j}^{\dagger} \\ &= \sum_{j} \mathcal{L}(V_{j}\rho_{m}V_{j}^{\dagger}) - 2\sum_{j_{1},j_{2}} V_{j_{2}}V_{j_{1}}\rho_{m}V_{j_{1}}^{\dagger}V_{j_{2}}^{\dagger} + \sum_{j} V_{j}\mathcal{L}\rho_{m}V_{j}^{\dagger} \\ &\Rightarrow G^{2}\rho_{m} + 2G\rho_{m}G^{\dagger} + \rho_{m}G^{\dagger^{2}} + \sum_{j=1}^{N_{V}} \left(V_{j}\rho_{m}\{G,V_{j}\}^{\dagger} + \{G,V_{j}\}\rho_{m}V_{j}^{\dagger}\right) + \sum_{j_{1},j_{2}} V_{j_{2}}V_{j_{1}}\rho_{m}V_{j_{1}}^{\dagger}V_{j_{2}}^{\dagger} = \mathcal{L}^{2}\rho_{m}. \end{split}$$

This completes the proof.